Long-time dynamics and hydrodynamic correlations in quasi-two-dimensional anisotropic colloidal mixtures

José Ramón Villanueva-Valencia,[1,*] Jesús Santana-Solano,[2] Erick Sarmiento-Gómez,[3] Salvador Herrera-Velarde,[4] José Luis Arauz-Lara,[3] and Ramón Castañeda-Priego[1,†]

[1]*División de Ciencias e Ingenierías, Campus León, Universidad de Guanajuato, Loma del Bosque 103, 37150 León, Guanajuato, Mexico*

[2]*Cinvestav Unidad Monterrey, Parque de Investigación e Innovación Tecnológica, Apodaca, Nuevo León 66629, Mexico*

[3]*Instituto de Física "Manuel Sandoval Vallarta," Universidad Autónoma de San Luis Potosí, Alvaro Obregón 64, 78000 San Luis Potosí, S.L.P., Mexico*

[4]*Subdirección de Postgrado e Investigación, Instituto Tecnológico Superior de Xalapa, Sección 5A Reserva Territorial s/n, 91096 Xalapa, Veracruz, Mexico*

(Received 9 July 2018; revised manuscript received 27 September 2018; published 10 December 2018)

The physical properties of multicomponent anisotropic colloidal dispersions are still far from being fully understood. This is mainly due to the fact that dealing with nonspherical particles and highly directional interactions is, from both experimental and theoretical points of view, a complicated task. In fact, experiments are scarce, and we still lack of model colloidal dispersions that allow us to simultaneously simplify and capture the complexity of such systems. In this contribution, we report on an experimental study of the hydrodynamic correlations and the long-time dynamics in anisotropic colloidal mixtures. The latter are composed of monomers and dimers highly confined between two parallel walls. The diffusive behavior is studied from low to intermediate particle concentrations. As concentration increases, crowding plays a significant role on the translational and rotational diffusion coefficients of monomers and dimers at short and long times. Nevertheless, in the short-time regime, the ratio between the dimer diffusion coefficients, parallel and perpendicular to the main axis of the dimer, becomes independent on the composition and total packing fraction; it depends only on the two translational hydrodynamic friction coefficients of the dimer. At long times, the dimer mean-square displacements, both parallel and perpendicular, reach the same value; i.e., the long-time diffusion coefficients seem not to be sensitive to the particle anisotropy and the crowded environment at which the dimer diffuses. Interestingly, both dynamical scenarios are analogous to the reported case for an isolated ellipsoid of similar dimensions, even though the dimer experiences collisions and hydrodynamic interactions with monomers and other dimers. Our findings also point out that the two-dimensional hydrodynamic correlations, monomer-monomer and monomer-dimer, differ mainly at short distances due to the difference in the shape of both types of species. However, contrary to the case of particles in a three-dimensional unbounded fluid, such hydrodynamic correlations decay faster, exhibiting a dipole-like long-ranged behavior with a r^{-2} dependence, similar to the results previously reported for a monodisperse quasi-two-dimensional colloidal dispersion. Our measurements are corroborated by means of molecular dynamics computer simulations that explicitly include the information of the host solvent.

DOI: 10.1103/PhysRevE.98.062605

I. INTRODUCTION

Nowadays, the study of the dynamics and structural properties of multicomponent colloidal systems has become a growing and active research area due to its importance for several interdisciplinary fields, such as medicine and biophysics, and its direct applicability in the industrial sector, for example, in the pharmaceutical and food industries [1–10].

In the bulk, i.e., far from any physical boundary, the available theoretical descriptions for colloidal particles interacting with radially symmetric potentials provide a good description of the whole dispersion [11]. These theoretical approximations allow us to understand and predict complex physical phenomena, such as phase equilibria, self-assembly, gelation, and the glass transition [12–21]. However, some efforts have been done to explore the richer dynamics and structure that naturally emerge in colloidal systems composed of particles without symmetry in their shape or interaction. When such degrees of freedom play a role, for example, the orientational ones, the colloidal dispersion may exhibit an intriguing phase behavior, such as the transition from an isotropic liquid state to a nematic or smectic phase [22–24].

In addition, when the motion of colloids is highly limited in one or more spatial dimensions, confinement adds new features to the dispersion due to the presence of constrictions, i.e., walls or immobile entities, that affect both the direct and hydrodynamic interactions between colloidal particles and, consequently, the transport properties [25–31].

The dynamical properties of colloidal dispersions are governed by the combination of both direct and indirect interactions [11]. The latter, typically known as hydrodynamic interactions (HIs), are always present because they are

*r.villanueva@fisica.ugto.mx
†ramoncp@fisica.ugto.mx

mediated by the host solvent. HIs strongly depend on the particle configuration and exhibit a long-ranged behavior [32]. These features increase the complexity of any theoretical approximation for the colloidal dynamics that includes explicitly the HI contribution [31,33]. In particular, computer simulations have shown that the inclusion of hydrodynamic tensors (for spherical particles) or the explicit incorporation of solvent molecules are able to reproduce experimental results of both isotropic and anisotropic colloidal systems at finite concentrations [34,35]. Recent studies on monodisperse spherical colloidal particles have shown that the contribution of HIs to the particle dynamics seems to be more important in the short-time regime [36,37].

Currently, it is a modern topic of discussion the relevance of HIs on the particle diffusion in the long-time regime [38,39]. Thorneywork *et al.* [40] claim that for monodisperse and bidisperse two-dimensional (2D) colloidal hard-sphere fluids, the long-time diffusivity is only a function of both the total packing fraction and the structural properties (through the value of the pair correlation function at contact). However, although this approximation seems to work well for spherical particles, it is not clear whether this result can be extended to a mixture of nonspherical particles because in this case one should consider both the orientational degrees of freedom and the nonisotropic interaction among colloids in order to properly account for the colloidal dynamics at all timescales [30].

In a previous work [34], we already contributed to the understanding of the effects of HIs on the short-time dynamics of mixtures of isotropic (spherical) and anisotropic (dumbbell-shaped) colloidal particles under severe confinement. Interestingly, we found that the contribution of HIs on the short-time diffusion coefficient of both species is the same and then can be factorizable in a wide range of concentrations, going from the dilute regime to high concentrations close to the spontaneous crystallization [34].

Hence, one of the aims of this work is to study the particle diffusivity in anisotropic colloidal mixtures highly confined between two glass plates; motion in the perpendicular direction to the plates is basically suppressed. We extend our previous work by presenting a more detailed study of the effective hydrodynamic correlations among particles and the long-time diffusion coefficients of the mixture. In the case of the dimers, the long-time diffusion coefficient can be decomposed into motions parallel and perpendicular to the main axis of the dimer, and hydrodynamic correlations between single monomers and monomers belonging to the dimers are determined as a function of the interparticle distance. The measurements are corroborated using molecular dynamics simulations, where HIs are taken into account by considering an explicit solvent that matches the experimental conditions.

II. EXPERIMENTAL SETUP

The experimental setup was previously introduced in Ref. [34]. To prepare colloidal dimers, polystyrene (spherical) particles of diameter $\sigma = 2$ μm in water solution (Duke Scientific) with negatively charged sulphate end groups on the surface are dialyzed against ultrapure water. Particle aggregation was promoted by the addition of salt. After 6 minutes, aggregation was quenched by dialysis of the colloidal suspension in clean water, and sinterization of particles in contact was induced by heating the suspension at a temperature close to the melting temperature of polystyrene [41–43]. After equilibrating the sample at room temperature, the different colloidal clusters are separated by centrifugation. The resulting dimers are now mixed with monomers and a small amount of larger particles of diameter 2.98 μm that serve as spacers. The colloidal dispersion is confined between two immobile and clean glass plates. Finally, the colloidal system is sealed with epoxy resin, and the mobile particles are allowed to equilibrate in the confined geometry [44,45].

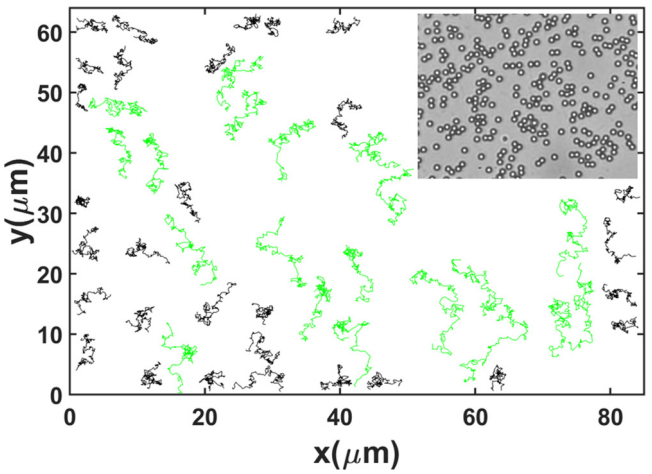

FIG. 1. Main panel: sample trajectories of the CM of dimers (black; shorter trajectories) and monomers (green; longer trajectories), relative to the fixed laboratory frame, with a time step of 0.5 s recorded in a time window of 100 s. Inset: Optical microscopy image for a monomer-dimer mixture with a dimer molar concentration of $x_d = 0.418$ and total area fraction $\phi = 0.118$. Dimers are identified by monitoring the average distance between adjacent particles as a function of time; see, e.g., Refs. [34,47].

The tracking procedure follows the standard method in optical video microscopy [46]. The sample is observed from a top view, i.e., perpendicular to the glass walls, using an optical microscope with a 40× objective and numerical aperture 0.6. The time evolution of the translational and rotational motions of colloids are recorded using a CCD camera at a rate of 30 frames per second, thus giving a temporal resolution of $\Delta t = 1/30$ s. Due to the high confinement of the mixture, the motion of the particles perpendicular to the walls is highly suppressed. Individual images extracted from the recorded video are analyzed to obtain both x and y coordinates of the center of the particles relative to the fixed laboratory frame, and from such data the trajectories are fully recovered; see Fig. 1. Dimers are identified by monitoring the average distance between adjacent particles as a function of time [34,47].

In order to explore a wide number of points in the parameter space (see Fig. 1 in Ref. [34]), the previous protocol is carried out for several values of the dimer molar concentration $x_d = 2N_d/N$, i.e., the number concentration of dimers, and total packing or surface fraction $\phi = NA_c/A$, i.e., the fraction of area occupied by the colloids, where N_d is the average

TABLE I. Representative experimental samples used to study the long-time dynamics and hydrodynamic correlation functions in binary mixtures of monomers and dimers.

Number of sample	Dimer molar concentration x_d	Surface fraction ϕ_{area}	Average number of colloids N
1	0.031	0.432	752
2	0.248	0.291	505
3	0.418	0.118	214
4	0.734	0.142	258

number of dimers, N is the average total number of colloids, A_c is the area of a colloid, and A is the total area of the view field (see inset of Fig. 1). ϕ and x_d are the control parameters that allows us to explore the effects of the concentration and composition, respectively. In particular, we have selected four representative experimental samples that serve us to explore the dynamical behavior at the long-time scale and the hydrodynamic correlations of the mixture with and without the dominant presence of dimers in the solution; see Table I.

III. LONG-TIME DYNAMICS

In the bulk, the theoretical formulation of diffusive motion of a spherical particle of diameter σ immersed in a solvent predicts that the self-diffusion coefficient, D^0, is determined by the thermal energy and viscosity of the host solvent [48]. Nonetheless, in the presence of other neighboring colloidal particles, the diffusive response of each particle is affected by both direct and indirect interactions [31,33]. As a consequence, the colloid dynamics follows a more complex behavior that is governed by the way in which particles interact directly or indirectly with each other.

One of the most fundamental observables in colloidal dynamics is the so-called *mean-square displacement* (MSD) [49]. This quantity is defined as the second moment of the distribution of particle positions,

$$W(t) = \langle [\vec{r}(t) - \vec{r}(0)]^2 \rangle, \tag{1}$$

where $\vec{r}(t)$ is the position of a particle at time t and $\langle \cdots \rangle$ denotes the ensemble average. The MSD is commonly used to characterize the dynamical time scales explored by a tracer particle in a colloidal dispersion. In open systems and at finite concentration, two timescales are typically observed within the diffusive regime [50,51]:

(1) The *short-time* regime, $\tau_B \ll t \ll \tau_I$, where τ_B is the characteristic time of the momentum relaxation and τ_I is the time at which a colloid has diffused over several layers of neighbors, i.e., when direct interactions between particles become important. Then, in this time regime, the colloids do not change appreciably their current configuration and each particle is caged by their neighboring particles, and it can diffuse only a short distance compared with its size. This dynamical regime is identified by the short-time diffusion coefficient for species i, D_i^s, with $W(t) = 2dD_i^s t$, where d is the dimensionality of the system. For $t < \tau_B$, the colloidal motion becomes ballistic: $W(t) \sim t^2$.

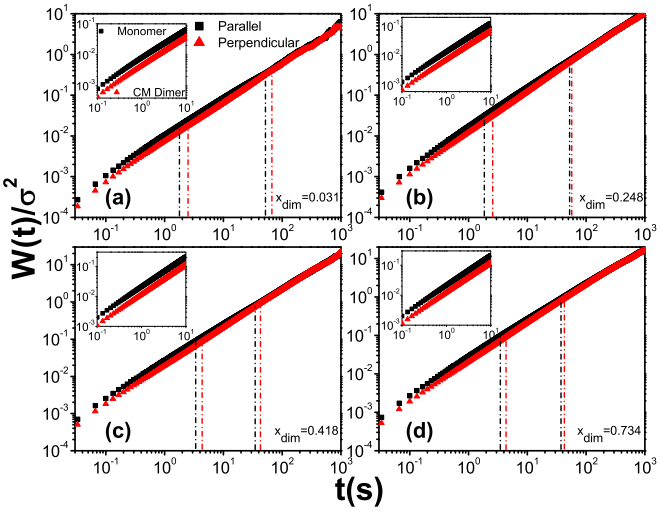

FIG. 2. Main panels (a–d) MSD parallel and perpendicular to the main axis of a dimer, relative to the fixed laboratory frame, for four representative samples at different packing fraction ϕ and molar concentration x_d (Table I). In the short-time regime, the MSD component parallel to the main axis of a dimer (filled squares) shows a faster dynamics than the perpendicular one (filled triangles). In the long-time regime, both parallel and perpendicular components collapse on the top of each curve, leading to the same long-time self-diffusion coefficient (see Table II). Insets (a–d) MSD for the CM of a monomer (upper curve; filled black squares) and CM of a dimer (lower curve; filled red triangles) from short- to long-time regimes. Vertical dashed-dotted lines in main panels (a–d) define the intermediate time window.

(2) The *long-time* regime, at $t \gg \tau_I$, where the colloidal particle experiences direct interactions with the neighboring particles and is able to escape from its initial cage; at this scale, the colloid has moved a distance that is several times the mean particle distance. This dynamical regime is identified by the long-time diffusion coefficient for species i, D_i^l, with $W(t) = 2dD_i^l t$.

From the experimental trajectories, obtained relative to the laboratory frame, the MSDs of the center of mass (CM) of monomers and dimers are determined. A tracer monomer is able to diffuse from one cage of neighboring particles to another, testing its dynamical transition from short- to long-time scales. On the other hand, the dimer is a rigid anisotropic body composed by a couple of joined spheres. As a result, its motion shows a more complex dynamical behavior, since there appears a coupling between both translational and rotational degrees of freedom caused by the fact that the interaction of the dimer with other particles is not radially symmetric.

In particular, the short-time diffusion coefficient for the CM of a monomer D_m^s, obtained through Eq. (1), is bigger than the short-time diffusion coefficient for the CM of a dimer D_d^s (see Table II). This behavior is observed in all the experimental samples (insets in Fig. 2) and agrees with previous experimental results [34]. The short-time dynamics is where apparently the long-ranged HIs show their major effects [32,52,53] and are more evident when concentration starts playing a role. This can also be seen in Table II; when ϕ increases, both D_m^s and D_d^s decrease due to the contribution of

TABLE II. Short-time (s) and long-time (l) diffusion coefficients for the CM of a monomer (m) and CM of a dimer (d). Ratio between the parallel ($\parallel$) and perpendicular ($\perp$) diffusion coefficients at short- and long-time scales. Last two rows show the short-time, $D^s_{\rm ang}$, and the long-time, $D^l_{\rm ang}$, angular diffusion coefficients, respectively.

Diffusion coefficient	Sample 1 $\phi = 0.432$	Sample 2 $\phi = 0.291$	Sample 3 $\phi = 0.118$	Sample 4 $\phi = 0.142$
D^s_m/σ^2 (s^{-1}) $\times 10^{-2}$	0.84 ± 0.02	1.36 ± 0.04	2.10 ± 0.06	2.13 ± 0.04
D^l_m/σ^2 (s^{-1}) $\times 10^{-2}$	0.45 ± 0.07	1.04 ± 0.03	1.95 ± 0.01	1.67 ± 0.02
D^s_d/σ^2 (s^{-1}) $\times 10^{-2}$	0.46 ± 0.01	0.73 ± 0.02	1.15 ± 0.03	1.21 ± 0.04
D^l_d/σ^2 (s^{-1}) $\times 10^{-2}$	0.23 ± 0.05	0.56 ± 0.04	1.02 ± 0.01	0.91 ± 0.03
$D^s_\parallel/D^s_\perp$	1.434 ± 0.054	1.402 ± 0.078	1.391 ± 0.057	1.408 ± 0.063
$D^l_\parallel/D^l_\perp$	1.077 ± 0.192	1.040 ± 0.036	0.994 ± 0.019	1.054 ± 0.015
$D^s_{\rm ang}$ ($rad^2 s^{-1}$) $\times 10^{-2}$	2.22 ± 0.01	2.79 ± 0.01	3.88 ± 0.01	4.13 ± 0.01
$D^l_{\rm ang}$($rad^2 s^{-1}$) $\times 10^{-2}$	1.91 ± 0.03	2.52 ± 0.02	3.71 ± 0.01	4.03 ± 0.02

the HIs, but also the area available to the dimers diminishes. As a consequence, dimers experience a hindered motion, which leads to a decrease in D^s_d due to crowding [34].

In the case of the dimers, the translational MSD can be decomposed into the parallel and perpendicular directions along the main axis of symmetry. The decomposition of the movement of the dimers in their parallel $\parallel$ and perpendicular $\perp$ components offer us a richer dynamical landscape. The main panels in Fig. 2 exhibit the full MSD behavior for the time window spanning from the short- to the long-time regime. In the short-time regime, $t \sim 10^{-1}$ s, the parallel movement of the dimer is faster than the perpendicular motion because the cross section of the former is smaller than the latter, implying that the probability of collision with the solvent molecules is reduced along that direction. A noteworthy observation is that the ratio between the parallel and perpendicular short-time diffusion coefficients ($D^s_\parallel/D^s_\perp$) in all samples is almost the same and thus is unlikely to be related with an HI effect (Table II). This point was recently reported and discussed by us in Ref. [34], but there we were not able to provide a satisfactory answer related with the physical mechanism responsible for such observation. However, we have carefully analyzed the friction coefficient that a dimer experiences in each direction (parallel and perpendicular). Through a 2D finite element calculation using ComSol Multiphysics 4.2®, which allowed us to solve the Navier-Stokes equation for the flow field in the vicinity of the dimer, we find that the ratio between both friction coefficients is around 1.45. This result is in good agreement with the experimental ratio $D^s_\parallel/D^s_\perp$ reported in Table II and agrees well with the experiments previously reported by Han *et al.* for the case of isolated ellipsoids with aspect ratio approximately to 2 [54].

As the time evolves, the dimer reaches a subdiffusive dynamical behavior at intermediate timescales. This time window can be calculated using the same procedure as in Ref. [55] and is denoted as vertical dotted lines in Fig. 2. After such a timescale, the parallel and perpendicular components of the MSD collapse on the top of each curve in the long-time regime, $t \sim 10^3$ s. The collapse of the parallel and perpendicular components of the MSD was first observed and reported in Ref. [56] for the Brownian motion of an ellipsoid under confinement. However, such a dynamical behavior might not be entirely expected in the case of an anisotropic binary mixture at finite concentration because, as discussed above, the difference in the cross sections, parallel and perpendicular, had allowed us to understand the distinction (or asymmetry) between both diffusion coefficients at short times as result of the HIs and crowding. However, we now observe that the long-time diffusion coefficients seem not to be sensitive to the particle anisotropy and the local environment at which the dimer diffuses. Nevertheless, such collapse can be related with the rotational diffusion of the particle during the time lapse where the translational MSD is analyzed. As the dimer also undergoes Brownian rotational motion, and in the long-time regime such rotation is large enough to complete a full rotation, decomposition of the MSD in parallel and transversal motion is pointless, giving exactly the same displacement in any direction; i.e., it becomes in an isotropic diffusive process at long times as has already been shown in Ref. [56].

We should point out that the system of Fig. 2(a) has poor statistics in the long-time regime due to the low dimer content; however, the MSD still follows the trend described in the previous paragraph. The experimental observation of the convergence of the parallel and perpendicular MSD at long times is confirmed through the determination of the ratio $D^l_\parallel/D^l_\perp \sim 1$ (Table II). The fact that this result is unaffected at low and high occupation of dimers implies that this is a ubiquitous result in the liquid phase. Nonetheless, it is also important to stress that the value of either $D^l_\parallel$ or $D^l_\perp$ decreases with the surface fraction, ϕ (see Table II).

As reported in Ref. [34], the molecular dynamics computer simulations (including the contribution of the host solvent) are able to capture the dynamics of the short-time regime. However, from a technical point of view, the long-time dynamics is difficult to reach. Thus, we do not show an explicit comparison between experiments and simulations in such time regime.

Figure 3 shows the mean-square angular displacement (MSAD) $W(t)_{\rm Ang} = \langle[\theta(t) - \theta(0)]^2\rangle$, of a dimer for the four samples in Table I, where $\theta(t)$ is the angle at time t that forms a line along the main axis of the dimer with the x axis of the laboratory frame [57]. The influence of the total packing fraction can be noticed in the behavior of the MSAD at short and long times; MSAD always decreases with ϕ. All curves are parallel, showing a uniform behavior at all timescales. Table II includes both, short-time, $D^s_{\rm ang}$, and long-time, $D^l_{\rm ang}$,

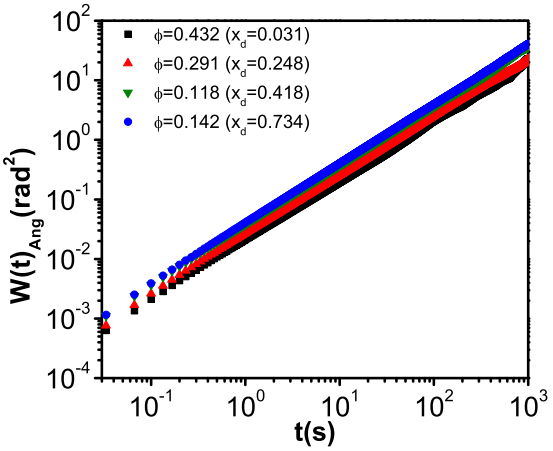

FIG. 3. MSAD of a dimer for four representative samples at different packing fraction ϕ and molar concentration x_d; see Table I. The angle is measured relative to the x axis of the fixed laboratory frame.

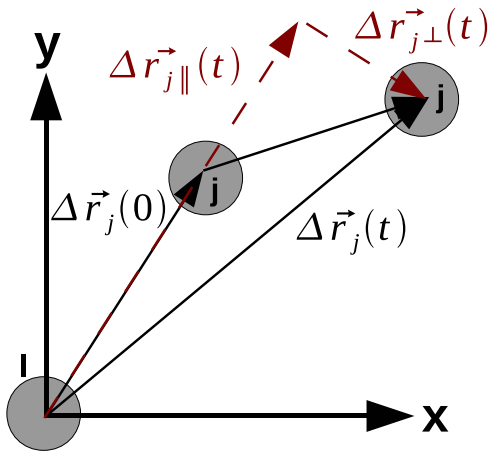

FIG. 4. Representation of the relative coordinate system. Schematic decomposition of $\Delta\vec{r}_j(t)$ on its parallel, $\Delta\vec{r}_{j\parallel}$, and perpendicular, $\Delta\vec{r}_{j\perp}$, components respect to the initial vector of separation $\Delta\vec{r}_j(0)$ between particles l (at the origin) and j; i.e., $\Delta\vec{r}_j(0)$ depends on the relative position of particles l and j at $t = 0$.

angular diffusion coefficients, whose values also depend on the particle concentration.

IV. HYDRODYNAMIC CORRELATIONS

HIs are long-ranged interactions, which cannot be screened or switched off completely and have contributions from all particles [58]. In a homogeneous three-dimensional (3D) colloidal system, the quantity that typically describes the hydrodynamic coupling between pairs of particles l and j in the presence of the other $N-2$ particles in the dispersion is the so-called hydrodynamic function [59]. The latter can be expressed in terms of the components of the *diffusion tensor*,

$$D_{lj}^{\alpha\beta}(t) = \frac{\langle \Delta r_l^{\alpha}(t)\Delta r_j^{\beta}(t)\rangle}{2t}, \tag{2}$$

with $\Delta r_l^{\alpha}(t) = r_l^{\alpha}(t) - r_l^{\alpha}(0)$ being the displacement of the particle l in the α direction relative to the laboratory frame. As demonstrated in Refs. [60,61], even for quasi-2D monodisperse and bidisperse mixtures composed of spherical particles, the hydrodynamic correlations keep the same functional form as their 3D counterpart. Here Eq. (2) is used to describe the hydrodynamic correlations between particles of the anisotropic quasi-2D mixture.

A. Experimental results

We now focus on the hydrodynamic correlations between a monomer and each of the two spheres of the dimer. With this information at hand, one can estimate the 2D hydrodynamic diffusion coefficients and quantify the contribution of the indirect interactions on the dynamical properties of the mixture. Usually, it is more convenient to describe the coupled motion of a pair of particles in terms of a relative $\vec{r} = \vec{r}_l - \vec{r}_j$ and a collective $\vec{c} = \vec{r}_l + \vec{r}_j$ coordinate system. Furthermore, relative and collective modes can be decomposed into parallel, $\parallel$, and perpendicular, $\perp$, components relative to the vector joining a pair of particles at time $t = 0$. Figure 4 exemplifies the decomposition of the relative coordinate system in parallel and perpendicular components to obtain the hydrodynamic correlation between particles l and j at different time steps. The collective coordinate system (figure not shown) is decomposed in a similar way. This implies that the hydrodynamic coupling between pairs of spheres is well described by four diffusion coefficients: collective parallel, $D_{c,\parallel}$, collective perpendicular, $D_{c,\perp}$, relative parallel, $D_{r,\parallel}$ and relative perpendicular, $D_{r,\perp}$ [60,61].

In order to measure all the hydrodynamic correlations from the experimental samples, the hydrodynamic diffusion coefficients are obtained in the linear time regime of the dynamical evolution of the colloids [$W(t) \propto t$]. We particularly have selected a time $t = 5\Delta t$. Our choice for the time $t = 5\Delta t$ (∼0.17 s) is mainly based on the fact that, at such time, the configuration of the particles has not exhibited an appreciable change; i.e., this time is much smaller than the time required for a particle to diffuse a distance equal to its diameter (∼120 s). However, technically speaking, this selection also reduces the spatial error attributed to particle tracking, which can greatly affect the results at very short times.

As one can see in Fig. 5, the four modes for (1) monomer-monomer correlation (filled symbols) and (2) monomer-dimer's sphere correlation (open symbols) present a very rich behavior; the modes display a higher correlation between particles at short distances, and, in general, they decay with the distance except for the relative parallel configuration at a distance of 2.3, which is more sensitive to particle concentration, but they are always present even for distances as large as six monomer diameters, giving rise to a very long-ranged interaction. Both sets of hydrodynamic diffusion coefficients, (1) and (2), exhibit similar trends when comparing similar modes. However, at distances less than two particle diameters, the diffusion coefficient for the second case is slightly reduced particularly for the relative modes. To our best understanding, this effect might be due to a hydrodynamic screening caused by the presence of the second particle of the dimer. In all samples, perpendicular components (collective and relative)

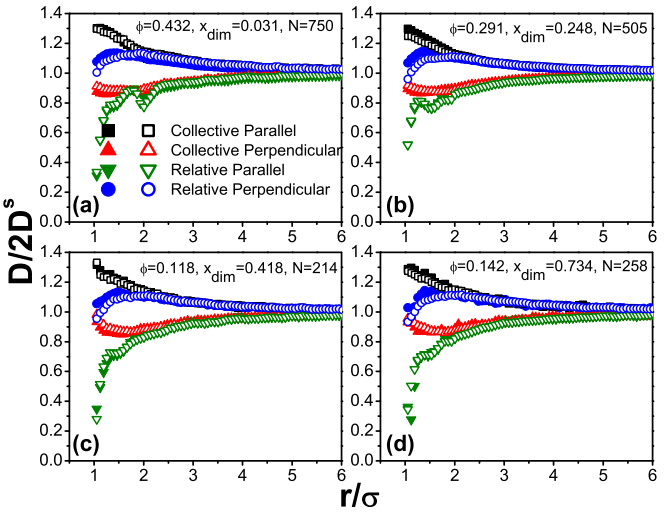

FIG. 5. Normalized experimental hydrodynamic diffusion coefficients vs radial distance between the center of each sphere for monomer-monomer (filled symbols) and monomer-dimer's sphere (open symbols) correlations.

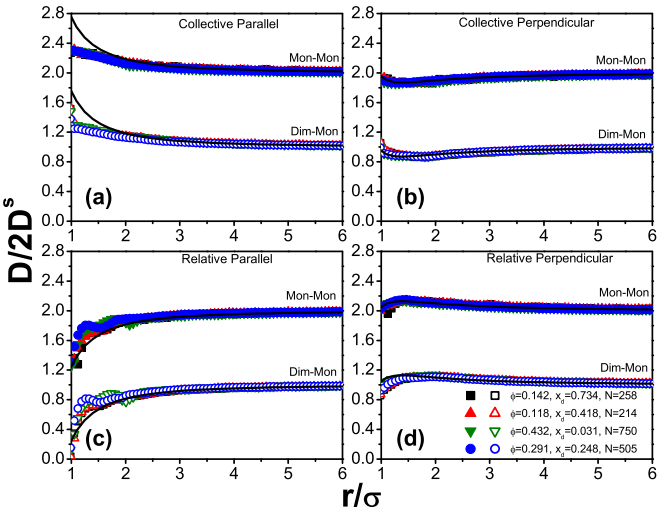

FIG. 6. (a–d) Asymptotic behavior of the four modes for monomer-monomer (solid symbols, shifted 1 unit) and monomer-dimer's sphere (open symbols) hydrodynamic correlations (same as Fig. 5). Solid lines in (b) and (d) are given by Eq. (3) with $a = 0.73$ and $b = 0.92$, while in (a) and (c) they are described by the function $\pm 0.73\,(r/\sigma)^{-2}$.

are highly symmetric, as can be seen in Fig. 5. Those correlations look like to be mirrored when compared with each other, while, in clear contrast, parallel components do not keep this trend for short interparticle distances ($r/\sigma < 2.5$). Additionally, the relative parallel component is the most affected by variations on the packing fraction, ϕ, and molar concentration of dimers, x_d, in particular, in the interval $1.0 < r/\sigma < 2.5$. This behavior has also been reported in similar colloidal systems (see, e.g., Refs. [60–63]), and such phenomenology is captured by the MD simulations, as we will see further below.

One of the most important features of the experimental findings shown in Fig. 5 is that for all parallel hydrodynamic coefficients, $D_{c,\parallel}/2D^s > 1$ and $D_{r,\parallel}/2D^s < 1$ implying that $(D_{c,\parallel} - D_{r,\parallel})/2D^s > 0$. Because parallel motions are positively correlated, the movement of one colloidal particle tends to drag another colloid in the same direction [61]. In contrast, for all perpendicular hydrodynamic coefficients $D_{r,\perp}/2D^s > 1$ and $D_{c,\perp}/2D^s < 1$, implying that $(D_{c,\perp} - D_{r,\perp})/2D^s < 0$, suggesting that the perpendicular motions are negatively correlated, and thus the movement of one colloidal particle causes an antidrag motion on the neighbor colloid. The same behavior can be inferred from the computer simulation results, as we discuss later. This information, which is not available by calculating any another dynamical quantity, shows the importance of estimating the hydrodynamic diffusion coefficients.

In quasi-2D colloidal systems, experimental evidence shows that the hydrodynamic interactions between spherical particles are long-ranged and decay as r^{-2} [62–64]. As we mentioned above, the perpendicular modes show a symmetrical behavior. For this reason, using the same functional form reported in Ref. [60], the perpendicular hydrodynamic modes are fitted using the following expression:

$$\frac{D_\perp}{2D^s} = 1 \pm a\left[\frac{1}{(r/\sigma)^2} - \frac{b}{(r/\sigma)^3}\right], \tag{3}$$

where "+" stands for the relative and "−" for the collective perpendicular components, respectively. The fit of the experimental data leads to $a = 0.73$ and $b = 0.92$. These values are almost independent of the molar concentration and packing fraction at distances larger than $r/\sigma \sim 3.0$, as shown in Figs. 6(b) and 6(d). As parallel components have a strong dependence on composition and total concentration at short distances, Figs. 6(a) and 6(c) are fitted only considering the dipole contribution r^{-2} to the flow field to recover the long distance trend [64]. At short distances, $r/\sigma \sim 1.0$–3.0, the fitting does not match the experimental results; however, when the distance increases, $r/\sigma > 3.0$, the agreement is better.

B. Computer simulation results

To further understand the experimental results, we have performed MD simulations of the whole colloidal dispersion taking into account explicitly the solvent molecules; one can include indirect interactions mediated by the host medium and, hence, elucidate the hydrodynamic interactions among particles [65]. The simulation results have been produced with the open source MD package ESPResSo [66,67]. In the simulations, we have considered a 2D system made up of monomers and dimers in a bath of smaller particles representing the solvent molecules. Dimers are formed using the rigid bond feature of ESPResSo [66,67]. All particles interact through a generalized version of the Lennard-Jones potential using the parameters of the pseudo-hard-sphere model recently proposed by Jover *et al.* [68]. Solvent particles have a diameter 10 times smaller than the colloidal particles and occupy a surface fraction that allows us to match the experimental conditions. We also explore the dynamics of the mixture using a finer representation of the coarse-grained solvent; we decreased the solvent size down until 20 times the colloidal particle. However, it was found to give the

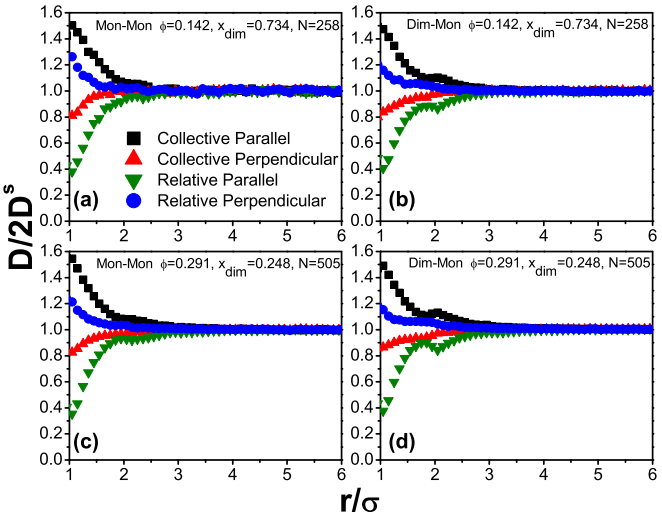

FIG. 7. Normalized hydrodynamic diffusion coefficients vs radial distance calculated from MD simulation results for surface fractions and dimer molar concentrations similar to the experimental samples 2 and 4 in Table I. (a, c) Monomer-monomer hydrodynamic correlation. (b, d) Monomer-dimer's sphere hydrodynamic correlations.

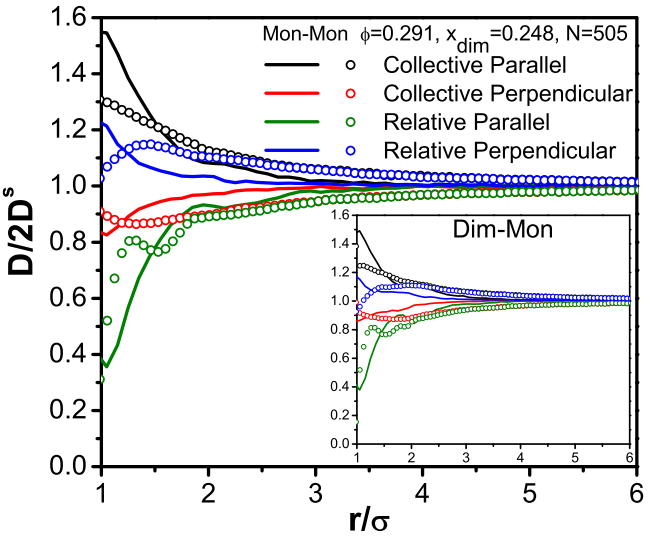

FIG. 8. Comparison between the hydrodynamic diffusion coefficients monomer-monomer obtained from MD computer simulation (lines) and the experimental counterpart (symbols) for sample 2 in Table I. Inset: Hydrodynamic diffusion coefficients dimer-monomer obtained from MD computer simulations (lines) and the experimental counterpart (symbols) for sample 2 in Table I.

same results but with an increase in computation time. At the beginning of the simulation, all particles are randomly distributed in the simulation box and during the simulation runs, the CM of each particle is constrained to move on the xy plane; i.e., motion along the z direction is not allowed. Simulations are performed in the NVT ensemble using the Langevin thermostat implemented in ESPResSo [66,67]. The total number of monomers and dimers used in the simulation matches the number of colloids observed in the field of view of the experiment; see Table I.

Figure 7 shows MD results for the hydrodynamic diffusion coefficients for a couple of samples to cover low and intermediate concentrations, samples 2 and 4 of Table I, respectively. The curves show that the hydrodynamic correlations decay faster than in the experiments, falling almost to zero at a distance of $r/\sigma \sim 3.0$, and exhibit stronger correlations at $r/\sigma \sim 1.0$. However, MD simulations are able to reproduce qualitatively the hydrodynamic correlation between particles found experimentally at the same order of magnitude, giving us confidence that our simulation model is able to emulate as first approximation the HIs, for example, the same symmetry in perpendicular components, the drag and antidrag behavior for parallel and perpendicular motions, respectively. Also, the strong dependence of the relative parallel configuration with the dimer molar concentration and packing fraction is well reproduced.

A more direct comparison between the experimental results and the computer simulations can be seen in Fig. 8 for the particular case of $\phi = 0.291$ and $x_{\rm dim} = 0.248$. The main figure shows the monomer-monomer hydrodynamic correlations, while the inset displays the monomer-dimer's sphere correlations. It is clear that simulation and experiment results do not match each other for all hydrodynamic correlations. The observed discrepancies between the experiment and MD results could be associated with the fact that we are considering a coarse-grained model for water molecules in two dimensions, while in the experiment water molecules fill a quasi-2D space. The fact that at short particle distances the coefficients in Fig. 8 exhibit a stronger correlation means that the solvent model is overestimated, whereas at larger distances the hydrodynamic is underestimated, giving rise to a short-range interaction between colloids. However, the effect of the HIs is nicely captured by the simulations; in the absence of "water molecules" this behavior cannot be simply observed. We should mention that MD simulations were carried out for all samples here considered, and the same qualitative agreement was obtained (data not shown). Nevertheless, further MD simulations are needed to better clarify the role of the composition on the hydrodynamic correlations among anisotropic colloids.

V. CONCLUDING REMARKS

In this work, the long-time dynamics and HI correlations in a quasi-2D binary colloidal mixture composed of monomers and dimers were experimentally studied. In particular, in the short-time regime, we proved that the ratio between the diffusion coefficients, parallel and perpendicular relative to the main axis of a dimer, $D^s_\parallel / D^s_\perp$, is around 1.40, a value theoretically confirmed by the numerical solution of the Navier-Stokes equation and associated with the ratio between both parallel and perpendicular friction coefficients. Furthermore, experimental evidence showed that at long times both MSDs, parallel and perpendicular, reach the same value; i.e., both long-time diffusion coefficients seem not to be sensitive to the particle anisotropy and the local environment at which the dimer diffuses. Both dynamical scenarios were analogous to the dynamics of a single ellipsoid, even though the diffusive behavior of the dimer was studied at finite concentrations; this is a regime where crowding might play a role, since

the dimer experiences multiple collisions and hydrodynamic interactions with monomers and other dimers that can affect its translational and rotational dynamics at all timescales.

We also observed that the 2D hydrodynamic diffusion coefficients, monomer-monomer and monomer-sphere of a dimer, differed only at short distances, finding also a long-ranged correlation that extends to distances as large as several diameters. Interestingly, both experiments and computer simulations exhibited the same symmetry in the perpendicular components, the drag and antidrag behavior for parallel and perpendicular motions, respectively, and the strong dependence of the relative parallel configuration with dimer molar concentrations and packing fractions. The experimental results were fitted using a dipolarlike relationship; that expression matched very well the long-ranged decay of the correlations, and its parameters, a and b, were independent of the composition and concentration. Expressions like Eq. (3) are clearly useful because they show that HIs between nonspherical particles can be easily modeled through an analytical function and serve to help us understand this complex contribution to the particle dynamics. They also allow us to build up a hydrodynamic tensor for anisotropic systems, which will be of great interest to study and predict additional features in the dynamical landscape of multicomponent nonspherical colloidal dispersions.

Last, but not least, we also observed that crowding played an important role for the translational and rotational diffusion coefficients of monomers and dimers at short and long times. Thus, it will be interesting to unravel the importance of the hydrodynamic interactions on the long-time dynamics of multicomponent anisotropic colloidal systems. Work along this line is in progress.

ACKNOWLEDGMENTS

The authors acknowledge to Dr. Angeles Ramírez-Saito for her technical support. This work was financially supported by CONACYT (Grants No. 237425, No. 287067 and No. 440 "Investigacion en Fronteras de la Ciencia 2015"). R.C.-P. also acknowledges the financial support provided by the Fundación Marcos Moshinsky and the Laboratorio Nacional de Ingeniería de la Materia Fuera de Equilibrio (Conacyt LN 294155 and Universidad de Guanajuato).

[1] J. G. Riess, J. Fluor. Chem. **114**, 119 (2002).
[2] Q. A. Pankhurst, J. Connolly, S. K. Jones, and J. Dobson, J. Phys. D: Appl Phys. **36**, R167 (2003).
[3] G. Cevc, Adv. Drug Deliv. Rev. **56**, 675 (2004).
[4] I. G. Denisov and S. G. Sligar, Chem. Rev. **117**, 4669 (2017).
[5] R. Homma, D. R. Johnson, D. J. Mc Clements, and E. A. Decker, Food Chem. **199**, 862 (2016).
[6] P. C. Mushenheim, J. S. Pendery, D. B. Weibel, S. E. Spagnolie, and N. L. Abbott, Proc. Natl. Acad. Sci. USA **113**, 5564 (2016).
[7] K. Maskaoui and J. L. Zhou, Environ. Sci. Pollut. Res. **17**, 898 (2010).
[8] D. J. Mc Clements, Curr. Opin. Colloid Interface Sci. **28**, 7 (2017).
[9] E. J. Yearley, P. D. Godfrin, T. Perevozchikova, H. Zhang, P. Falus, L. Porcar, M. Nagao, J. E. Curtis, P. Gawande, R. Taing *et al.*, Biophys. J. **106**, 1763 (2014).
[10] D. Vural, L. Hong, J. C. Smith, and H. R. Glyde, Phys Rev. E **88**, 052706 (2013).
[11] V. N. Manoharan, Science **349**, 1253751 (2015).
[12] E. Lázaro-Lázaro, P. Mendoza-Méndez, L. F. Elizondo-Aguilera, J. A. Perera-Burgos, P. E. Ramírez-González, G. Pérez-Ángel, R. Castañeda-Priego, and M. Medina-Noyola, J. Chem. Phys. **146**, 184506 (2017).
[13] G. Pérez-Ángel, L. E. Sánchez-Díaz, P. E. Ramírez-González, R. Juárez-Maldonado, A. Vizcarra-Rendón, and M. Medina-Noyola, Phys. Rev. E **83**, 060501(R) (2011).
[14] S. Mazoyer, F. Ebert, G. Maret, and P. Keim, Europhys. Lett. **88**, 66004 (2010).
[15] E. R. Weeks and D. A. Weitz, Phys. Rev. Lett. **89**, 095704 (2002).
[16] P. N. Pusey and W. van Megen, Nature (London) **320**, 340 (1986).
[17] G. Foffi, G. D. McCullagh, A. Lawlor, E. Zaccarelli, K. A. Dawson, F. Sciortino, P. Tartaglia, D. Pini, and G. Stell, Phys. Rev. E **65**, 031407 (2002).
[18] A. Stradner, H. Sedgwick, F. Cardinaux, W. C. K. Poon, S. U. Egelhaaf, and P. Schurtenberger, Nature (London) **432**, 492 (2004).
[19] M. Chiappini, E. Eiser, and F. Sciortino, Eur. Phys. J. E **40**, 7 (2017).
[20] E. P. Bernard and W. Krauth, Phys. Rev. Lett. **107**, 155704 (2011).
[21] S. C. Kapfer and W. Krauth, Phys Rev. Lett. **114**, 035702 (2015).
[22] H. E. Bakker, S. Dussi, B. L. Droste, T. H. Besseling, C. L. Kennedy, E. I. Wiegant, B. Liu, A. Imhof, M. Dijkstra, and A. van Blaaderen, Soft Matter **12**, 9238 (2016).
[23] C. Xia, K. Zhu, Y. Cao, H. Sun, B. Kou, and Y. Wang, Soft Matter **10**, 990 (2014).
[24] D. Chen, J. H. Porada, J. B. Hooper, A. Klittnick, Y. Shen, M. R. Tuchband, E. Korblova, D. Bedrov, D. M. Walba, M. A. Glaser *et al.*, Proc. Natl. Acad. Sci. USA **110**, 15931 (2013).
[25] B. Lin, J. Yu, and S. A. Rice, Phys. Rev. E **62**, 3909 (2000).
[26] B. Lin, J. Yu, and S. A. Rice, Coll. Surf. A **174**, 121 (2000).
[27] H. Brenner, Chem. Eng. Sci. **16**, 242 (1961).
[28] V. N. Michailidou, G. Petekidis, J. W. Swan, and J. F. Brady, Phys. Rev. Lett. **102**, 068302 (2009).
[29] L. F. Elizondo-Aguilera and M. Medina-Noyola, J. Chem. Phys. **142**, 224901 (2015).
[30] S. Vivek and E. R. Weeks, J. Chem. Phys. **147**, 134502 (2017).
[31] J. Happel and H. Brenner, *Low Reynolds Number Hydrodynamics* (Kluwer, Dordrecht, 1983).
[32] S. Herrera-Velarde, E. C. Euán-Díaz, F. Córdoba-Valdés, and R. Castañeda-Priego, J. Phys.: Condens. Matter **25**, 325102 (2013).
[33] J. K. G. Dhont, *An Introduction to Dynamics of Colloids* (Elsevier, Nethelands, 1996).
[34] E. Sarmiento-Gómez, J. R. Villanueva-Valencia, S. Herrera-Velarde, J. A. Ruiz-Santoyo, J. Santana-Solano, J. L. Arauz-Lara, and R. Castañeda-Priego, Phys. Rev. E **94**, 012608 (2016).

[35] A. Torres-Carbajal, S. Herrera-Velarde, and R. Castañeda-Priego, Phys. Chem. Chem. Phys **17**, 19557 (2015).
[36] A. L. Thorneywork, R. E. Rozas, R. P. A. Dullens, and J. Horbach, Phys. Rev. Lett. **115**, 268301 (2015).
[37] K. Zahn, J. M. Méndez-Alcaraz, and G. Maret, Phys. Rev. Lett. **79**, 175 (1997).
[38] M. Medina-Noyola, Phys. Rev. Lett. **60**, 2705 (1988).
[39] P. Holmqvist and G. Nägele, Phys. Rev. Lett. **104**, 058301 (2010).
[40] A. L. Thorneywork, D. G. A. L. Aarts, J. Horbach, and R. P. A. Dullens, Phys. Rev. E **95**, 012614 (2017).
[41] P. M. Johnson, C. M. van Kats, and A. van Blaaderen, Langmuir **21**, 11510 (2005).
[42] A. M. Yake, R. A. Panella, C. E. Snyder, and D. Velegol, Langmuir **22**, 9135 (2006).
[43] M. Ibisate, Z. Zou, and Y. Xia, Adv. Funct. Mater. **16**, 1627 (2006).
[44] M. D. Carbajal-Tinoco, R. López-Fernández, and J. L. Arauz-Lara, Phys. Rev. Lett. **99**, 138303 (2007).
[45] A. Ramírez-Saito, M. Chávez-Páez, J. Santana-Solano, and J. L. Arauz-Lara, Phys. Rev. E **67**, 050403(R) (2003).
[46] J. C. Crocker and D. G. Grier, J. Coll. Int. Sci. **179**, 298 (1996).
[47] A. García-Castillo and J. L. Arauz-Lara, Phys. Rev. E **78**, 020401(R) (2008).
[48] W. B. Russel, D. A. Saville, and W. R. Schowalter, *Colloidal Dispersions* (Cambridge University Press, Cambridge, 1989).
[49] N. G. van Kampen, *Stochastic Processes in Physics and Chemistry* (North-Holland, New York, 1981).
[50] A. J. Banchio and G. Nägele, J. Chem. Phys. **128**, 104903 (2008).
[51] G. Nägele and P. Baur, Physica A **245**, 297 (1997).
[52] G. Nägele, Phys. Rep. **272**, 215 (1996).
[53] J. C. Meiners and S. R. Quake, Phys. Rev. Lett. **82**, 2211 (1999).
[54] Y. Han, A. Alsayed, M. Nobili, and A. G. Yodh, Phys. Rev. E **80**, 011403 (2009).
[55] Z. Zheng and Y. Han, J. Chem. Phys. **133**, 124509 (2010).
[56] Y. Han, A. M. Alsayed, M. Nobili, J. Zhang, T. C. Lubensky, and A. G. Yodh, Science **314**, 626 (2006).
[57] G. Boniello, A. Stocco, M. Gross, M. In, C. Blanc, and M. Nobili, Phys. Rev. E **94**, 012602 (2016).
[58] D. J. Kraft, R. Wittkowski, B. ten Hagen, K. V. Edmond, D. J. Pine, and H. Löwen, Phys. Rev. E **88**, 050301(R) (2013).
[59] G. K. Batchelor, J. Fluid. Mech. **74**, 1 (1976).
[60] J. Santana-Solano, A. Ramírez-Saito, and J. L. Arauz-Lara, Phys. Rev. Lett. **95**, 198301 (2005).
[61] D. T. Valley, S. Rice, B. Cui, H. Diamant, and B. Lin, J. Chem. Phys. **126**, 134908 (2007).
[62] H. Diamant, B. Lin, and S. A. Rice, J. Phys.: Condens. Matter **17**, S2787 (2005).
[63] H. Diamant, B. Lin, and S. A. Rice, J. Phys.: Condens. Matter **17**, S4047 (2005).
[64] B. Cui, H. Diamant, B. Lin, and S. A. Rice, Phys. Rev. Lett. **92**, 258301 (2004).
[65] V. Pryamitsyn and V. Ganesan, J. Chem. Phys. **122**, 104906 (2005).
[66] H. J. Limbach, A. Arnold, B. A. Mann, and C. Holm, Comput. Phys. Commun. **174**, 704 (2006).
[67] A. Arnold, O. Lenz, S. Kesselheim, R. Weeber, F. Fahrenberger, D. Roehm, P. Košovan, and C. Holm, in *Meshfree Methods for Partial Differential Equations VI*, edited by M. Griebel and M. A. Schweitzer, Lecture Notes in Computational Science and Engineering Vol. 89 (Springer, Berlin, 2013), pp. 1–23.
[68] J. Jover, A. J. Haslam, A. Galindo, G. Jackson, and E. A. Müller, J. Chem. Phys. **137**, 144505 (2012).